Thermal-assisted synthesis of unique Cu nanodendrites for the efficient electrochemical reduction of CO_2

M. Nur Hossain, Shuai Chen, Aicheng Chen*

Electrochemical Technology Centre, Department of Chemistry, University of Guelph, 50 Stone Road East, Guelph, Ontario, N1G 2W1, Canada

ARTICLE INFO

ABSTRACT

Herein, we report on novel Cu nanodendrites, which were formed when the electrodeposited Cu thin film on a Ti substrate was thermally treated in the presence of a mixture of $CuSO_4$ and H_2SO_4. The formed Cu nanodendrites exhibit superior catalytic activity for the electrochemical reduction of CO_2, showing that the unique nanostructure and the large electrochemically active surface area play critical roles in the efficient electrochemical reduction of CO_2. Gas chromatography and NMR spectroscopy were employed to identify the products of the CO_2 reduction, confirming the formation of CO, CH_4, $HCOO^-$, CH_3COO^- and CH_3OH. The kinetics of the CO_2 reduction was further investigated using in situ electrochemical ATR-FTIR spectroscopy. The facile approach to the fabrication of the unique Cu nanodendrites, the superior catalytic activity, and the high current efficiency make the Cu nanodendrites as a promising electrocatalyst for the effective electrochemical reduction of CO_2 to valuable products.

1. Introduction

CO_2 is considered as one of the crucial greenhouse gasses and plays a vital role for the rising of global average temperature. The emission of CO_2 is mainly resulted from burning fossil fuels in industries, vehicles, household use and volcanic eruption. In addition, fossil fuels will be depleted due to the extensive and continuous use in the daily human life; and the world will face a severe challenge to mitigate the energy supply and production. Hence, there is an urgent need to find a sustainable energy source and to create a new way to use renewable energy. The conversion of CO_2 into fuels using electrochemical reduction could be one of the competent approaches as renewable energy generation [1,2]. Although various materials have been explored as electrocatalysts for the electrochemical reduction of CO_2 over the last a few decades, their performance is still not high enough for practical use in terms of both energy efficiency and stability [3–12]. Metal-based electrodes have been extensively used for electrochemical reduction of CO_2 [6–9]. Among them, copper-based materials have gained particular attention because these catalysts are capable of producing hydrocarbon fuel products such as formic acid (HCOOH), acetic acid (CH_3COOH), methanol (CH_3OH), methane (CH_4), ethane (C_2H_4) and so forth. However, it still requires high overpotential, which causes significant hydrogen evolution in an aqueous solution and results in a low Faradaic efficiency for CO_2 reduction [10–14]. For example, polycrystalline Cu

requires a higher than 0.5 V overpotential to achieve the current density of 1 mA cm^{-2} for the conversion of CO_2 to CO and HCOOH, and a more than 0.8 V overpotential to further reduce to CH_4 and C_2H_4 [13,14].

Different types of Cu electrodes have been explored towards the electrochemical reduction of CO_2 such as Cu plates, Cu foils, Cu coated gas diffusion electrodes, Cu electrodeposited glassy carbon electrodes, nanostructured Cu (e.g., nanowires, nanoflowers, nanofoams and nanopores), and copper-based alloys to overcome these boundaries [13,15–22]. The nanostructured Cu materials may possess a high surface roughness factor, a large EASA, and different crystal facets. Several studies have been carried out to understand the effect of these properties on the electrochemical reduction of CO_2; significant improvement has been achieved on the catalytic performance using the nanostructured Cu materials over the typical metal electrodes as an electrocatalyst for CO_2 reduction [10,23,24]. Recently, oxide-derived Cu (OD-Cu) nanomaterials have gained a wide attention as an efficient electrocatalysts toward the CO_2 and CO reduction [10,13,25–27]. The OD-Cu nanomaterials are made through electrochemical reduction of copper oxides, where coper oxides are formed by the thermal treatment of typical Cu nanoparticles (NPs). The thermal process could alter the surface structure of polycrystalline nanoparticles that might have an enhanced catalytic activity towards the CO_2 and CO reduction. The derived nanomaterials form interconnected nanocrystalline networks and exhibit small crystallite sizes as well as a large EASA and high

---

* Corresponding author.
  E-mail address: aicheng@uoguelph.ca (A. Chen).

roughness factor that favor C−C coupling formation during the electrochemical reduction of CO_2 and CO [10,13,25–29]. The formation of CO and HCOOH occurs at low overpotentials, whereas CH_4 and C_2 hydrocarbons are produced comparatively at a high overpotential during the electrochemical reduction of CO_2 on these OD-Cu nanomaterials [10,26,30]. It has also been known that the OD nanocrystalline Cu is more favorable to reduce CO to multi-carbon oxygenates in the potential range between −0.3 V and −0.7 V (vs. RHE) [25,27].

Moreover, great efforts have been made to investigate the kinetics of the electrochemical reduction of CO_2 on Cu electrodes [31–36]. In situ electrochemical attenuated total reflection Fourier-transform infrared (ATR-FTIR) spectroscopy is a powerful technique to probe the species consumed and produced during electrochemical processes. Recent studies indicate that CO is the primary species that adsorbed on the Cu electrode surface during CO_2 electrolysis, which also acts as the intermediate for the formation of other reduced products [32,33,37–40]. It is well-known that hydrogen evolution is the major cause of the low Faradic efficiency of the CO_2 reduction; however, there is no report on the in situ FTIR studies of the kinetics of water splitting and CO_2 reduction at a nanostructured electrode/electrolyte interface.

Herein, we have demonstrated unique Cu nanodendrites with a high EASA as an efficient electrocatalyst for CO_2 reduction. The nanodendrites were synthesized using a facile thermal-assisted approach; the effect of the precursors, calcination temperature and time on the formation of the Cu nanodendrites were systemically investigated. The optimized nanodendrites exhibit excellent catalytic activity for CO_2 reduction with a remarkable current efficiency. In situ electrochemical ATR-FTIR spectroscopy was employed for the first time to investigate the mechanism of the CO_2 reduction and the kinetics of the water splitting and CO_2 reduction at the Cu nanodendrites.
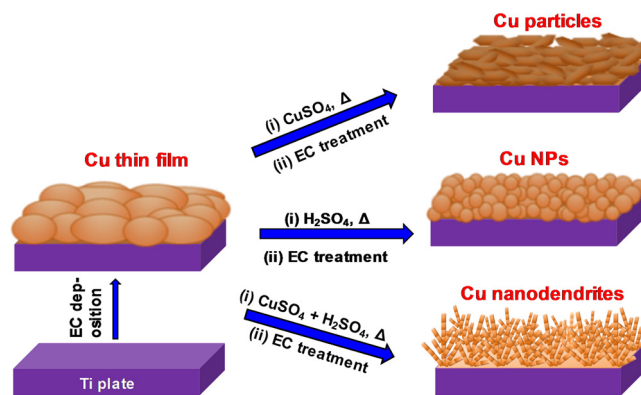
2. Experimental section

2.1. Chemicals and materials

$CuSO_4.5H_2O$ (99.999%), Na_2SO_4 (≥99.5%), H_2SO_4 (≥99.99%), D_2O (99.9 at.%), TMS (99.5%) and $NaHCO_3$ (≥99.0%) solutions were obtained from Sigma Aldrich; copper plate (99.9985%, 0.5 mm thick) was purchased from Alfa Aesar; the Ti substrates (99.2%, 1.25 cm × 0.80 cm ×0.5 mm) was purchased from Sigma Aldrich; carbon dioxide (99.999%) and Ar (99.995%) gases were purchased from Praxair. The CO_2 reduction was conducted in a CO_2-saturated 0.1 M $NaHCO_3$ electrolyte solution. Pure H_2O produced from a Nanopure Diamond™ UV ultrapure water purification system (18.2 MΩ cm) was used to prepare all the electrolyte solutions.

2.2. Fabrication of electrodes

A Ti plate (1.0 cm^2) served as a substrate was cleaned using acetone by an ultrasonic cleaner for 10 min followed by 10 min in pure H_2O, and then etched in 5.0 M HCl at approximately 85 °C for 20 min. Copper foils were etched for 1 min in 35% HNO_3 and washed out with a copious amount of deionized water, and then dried off with the flow of N_2 gas. Scheme 1 illustrates the preparation of the Cu thin film and different oxide-derived (OD) nanostructured Cu. In an attempt to the synthesis of different Cu nanostructures, Ti plate was used as the cathode, and the etched copper foil was served as the anode in a mixture of 0.1 M $CuSO_4$ and 0.5 M H_2SO_4 solution in a three-electrode cell system with an Ag/AgCl as the reference electrode. Cyclic voltammetry (CV) was employed in the potential window of 0.0 to −0.5 V (vs. Ag/AgCl) at the scan rate of 50 mV s^{-1} for 50 cycles to deposit copper on the Ti substrate, which is named as the Cu thin film (Scheme 1). The formed Cu thin film was annealed at 500 °C for 1 h followed by applying a cathodic current density of 10 mA cm^{-2} for 30 min in a CO_2-saturated 0.1 M $NaHCO_3$ solution (which is named as the EC treatment) to form the OD-Cu thin film. In order to form Cu particles and Cu nanoparticles, a 50 μL of

Scheme 1. Schematics of the preparation of the different Cu nanomaterials.

0.1 M $CuSO_4$ and a 50 μL 0.5 M H_2SO_4 were deposited on Cu thin film before the calcination, respectively; whereas a 50 μL of mixture of 0.1 M $CuSO_4$ and 0.5 M H_2SO_4 was cast on the Cu thin film to form the Cu nanodendrites (Scheme 1). The formation of the Cu nanodendrites was also optimized by changing the volume of the mixture from 30 to 70 μL, varying the calcination temperature from 400 to 600 °C, and altering the calcination time from 30 to 90 min.

2.3. Characterization of the synthesized Cu-based nanomaterials

Scanning electron microscopic (SEM) images and energy dispersive X-ray (EDX) analysis were performed using an FE-SEM (Hitachi SU-70) at 10.0 kV to study the morphologies, the structures and surface composition of the prepared electrodes. X-ray photoelectron spectroscopic (XPS) characterization was carried out with a Thermo Scientific XPS system, where the samples were adjusted to take-off angle of 90° (relative to the surface), and the spot size of the X-ray was 400 μm with an Al Kα monochromatic source. XPSPEAK 4.1 software was employed for all the data processing. The crystalline phase analysis was performed via a Phillips PW 1050-3710 with Cu Kα$_1$ of 1.54060 Å as the radiation source to record X-ray diffraction (XRD) patterns. The full range of 2θ data was taken with a step of 0.01°/2θ width. Scherrer Equation $L = 0.94\lambda/\beta \cos\theta$ (where λ denotes the Cu Kα radiation, and β corresponds to the full width at half-maximum for a reflection maximum) was employed to calculate the crystallite size (L) of each sample. To eliminate the strong XRD peaks derived from the substrate, the formed different Cu nanostructured coatings were scratched off from the Ti substrates. $L = \frac{0.94\lambda}{\beta\cos\theta}$ PANalytical X'Pert HighScore Plus software was used to analyze and fit the XRD data.

2.4. Electrochemical characterization

A CHI 660E workstation (CH Instrument Inc. USA) was operated for electrochemical study using CV, Linear sweep voltammetry (LSV) and chronoamperometry (CA) in a three-electrode cell system. A platinum coil (10.0 cm^2) was used as the counter electrode, which was cleaned via flame annealing and quenching with deionized H_2O before each experiment. The reference electrode used was an Ag/AgCl (3.0 M KCl) electrode and the measured electrode potential was converted to the reversible hydrogen electrode (RHE) scale (E vs. RHE) using the following equation:

E (vs. RHE) = E (vs. Ag/AgCl) + 0.0591 V × pH + 0.210 V

A CO_2-saturated 0.1 M $NaHCO_3$ solution with pH of 6.65 was used as the electrolyte for all the CO_2 reduction experiments.

2.5. Electrochemically active surface area (EASA) determination

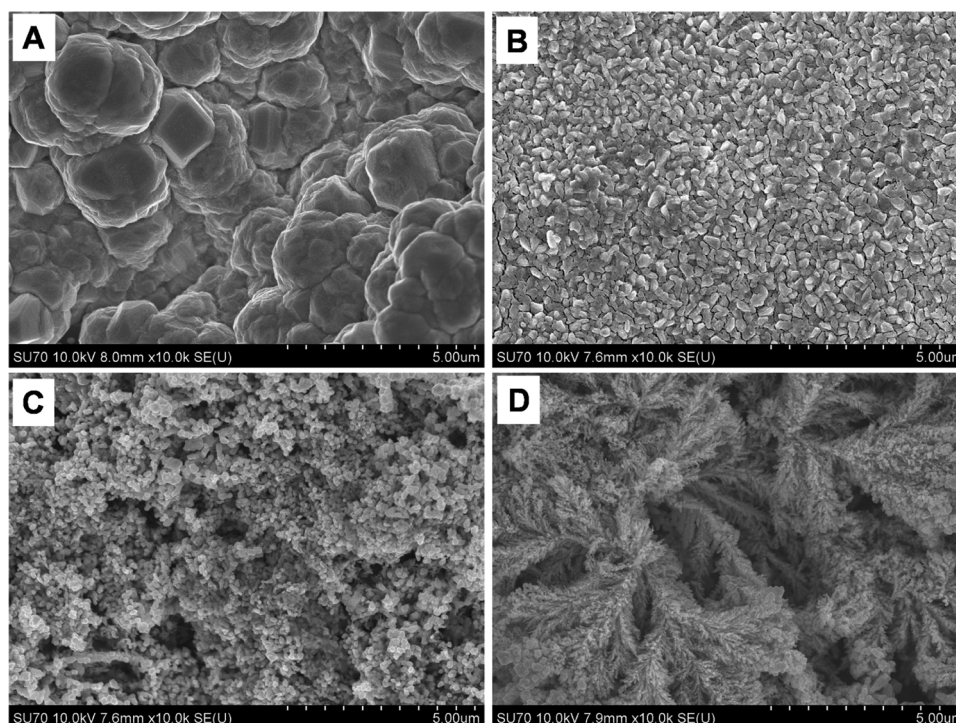Surface roughness factors of the formed Cu thin film, OD-Cu NPs

Fig. 1. SEM images of the electrochemical deposited Cu thin film (A), Cu particles (B), Cu nanoparticles (C), and Cu nanodendrites (D).

and Cu nanodendrites were estimated relative to a smooth Cu poly-crystalline electrode based upon their double-layer capacitances [27], where the CVs were recorded in a 0.1 M HClO$_4$ electrolyte. The potential windows were chosen in which no obvious Faradaic reactions occurred. The geometrical current densities versus the scan rate of the CV was plotted for each electrode and the capacitance was estimated from the slope of the linear regression.

2.6. In situ electrochemical ATR-FTIR study

The in situ electrochemical ATR-FTIR measurements were carried out using an 8700 Nicolet Fourier transform infrared spectrometers associated with a ZnSe window and a liquid N$_2$-cooled MCT detector. A spectro-electrochemical cell was made of Teflon, where synthesized Cu nanodendrites grown on Ti substrate acted as the working electrode and were in contact with the ZnSe hemisphere window (Scheme S1). A platinum coil and an Ag/AgCl (3.0 M KCl) were used as the counter electrode and the reference electrode, respectively. All interferograms were acquired at 4 cm^{-1} resolution; the resulting ATR-FTIR spectra were plotted in terms of the relative change of the electrode reflectivity and calculated using following equation [41]:

$$\Delta R/R = [R(E_2) - R(E_1)] / R(E_1)$$

where R(E$_1$) and R(E$_2$) are the reflectivities from the electrode surface at the applied potential E$_1$ and E$_2$, respectively. The spectrum recorded at E$_1$ = +0.2 V was used as the background.

2.7. Bulk electrolysis of CO$_2$

Electrochemical reduction of CO$_2$ was performed in a liquid-tight two-compartment cell with a cationic exchange membrane (CMI-7000S) as the separator at room temperature. The working electrode and the reference electrode (Ag/AgCl) were placed in the same compartment, where CO$_2$ was continuously purged during the electrolysis (to keep the 0.1 M NaHCO$_3$ solution always CO$_2$ saturated), and the other compartment contained the counter electrode (Pt coil) with the CO$_2$ saturated 0.1 M NaHCO$_3$ solution. Gas chromatography (GC,

Shimadzu GC-2014) was employed for analyzing the gas products generated from the CO$_2$ reduction. To identify the formed liquid products, a Varian Unity Inova 500 was employed to record the one-dimensional ^{1}H NMR spectra. A mixture of the electrolyte solution sample and 20% D$_2$O was used, where 0.05 μL TMS (tetramethylsilane) was added to the sample as the internal reference.

3. Results and discussion

3.1. Characterization of electrodes

Fig. 1 displays the SEM images of the different Cu nanostructures. A Cu thin film with some large crystalline was initially deposited on a Ti substrate via a facile electrochemical deposition method as seen in Fig. 1A. The formed Cu thin film was then calcinated at 500 °C for 1 h to form copper oxides. A rough surface of the Cu thin film was obtained after the EC treatment of the formed oxides (Fig. S1). As seen in Fig. 1B, Cu particles with ~500 nm were formed when the Cu thin film was coated with CuSO$_4$, calcinated at 500 °C for 1 h and followed by the EC treatment. A significant change by the formation of NPs (~100 nm) were observed when the Cu thin film was calcinated in the presence of H$_2$SO$_4$ (Fig. 1C), indicating that H$_2$SO$_4$ played as an etching agent to form the NPs. Interestingly, nanodendrites with tertiary branches were formed when the Cu thin film were modified with a mixture of CuSO$_4$ and H$_2$SO$_4$ and calcinated at 500 °C for 1 h (Fig. 1D), indicating that simultaneous formation and etching of Cu nanoparticles occurred during the calcination.

Fig. S2 depicts the EDX spectra of the formed copper oxides and Cu nanodendrites. Strong O and Cu peaks appeared in Spectrum (i) of Fig. S2, confirming that copper oxide nanodendrites were formed during the calcination. Fig. S3 displays the E – t curve during the EC treatment of the copper oxide nanodentrite electrode at the applied cathodic current of 10 mA cm^{-2} for 1000 s in a CO$_2$-saturated 0.1 M NaHCO$_3$ solution. The reduction of cupper oxides primarily occurred during the first 150 s, where the electrode surface was changed from black to copper color. Then the electrode potential stabilized at approximately −0.55 V (vs RHE), indicating the freshly formed Cu nanodendrites possessed
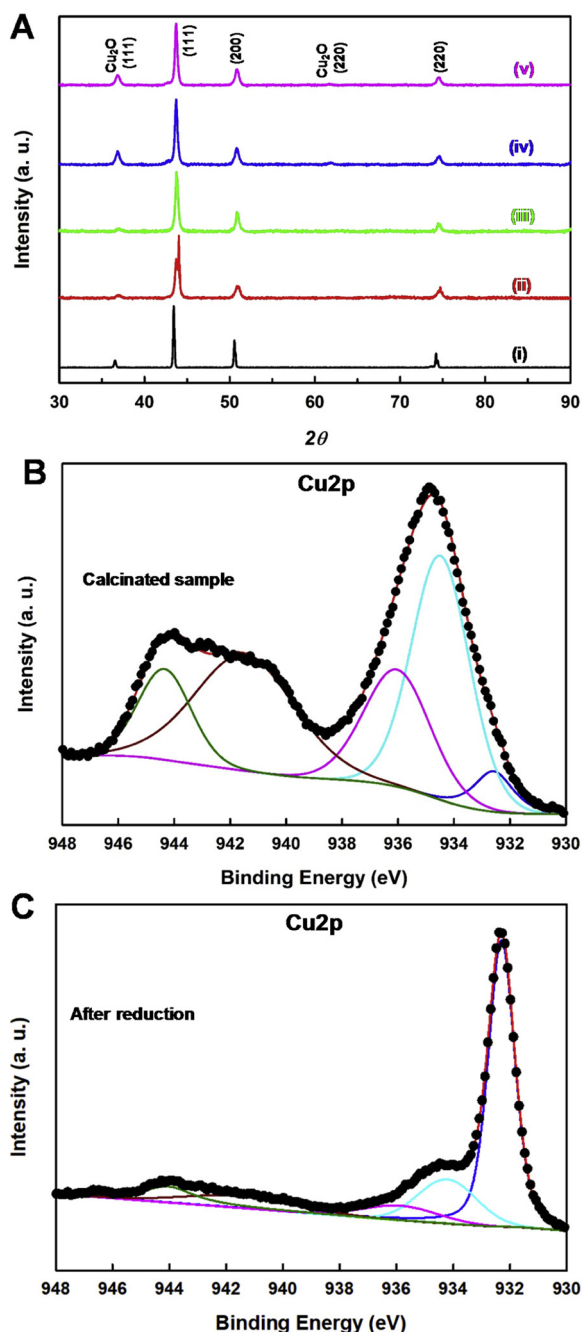
Fig. 2. (A) XRD spectra of the different Cu electrodes: (i) Cu thin film, (ii), OD-Cu thin film, (iii) Cu particles, (iv) Cu nanoparticles, (v) Cu nanodendrites; XPS spectra at the Cu2p region of copper oxides prior to (B) and after the EC treatment (C).
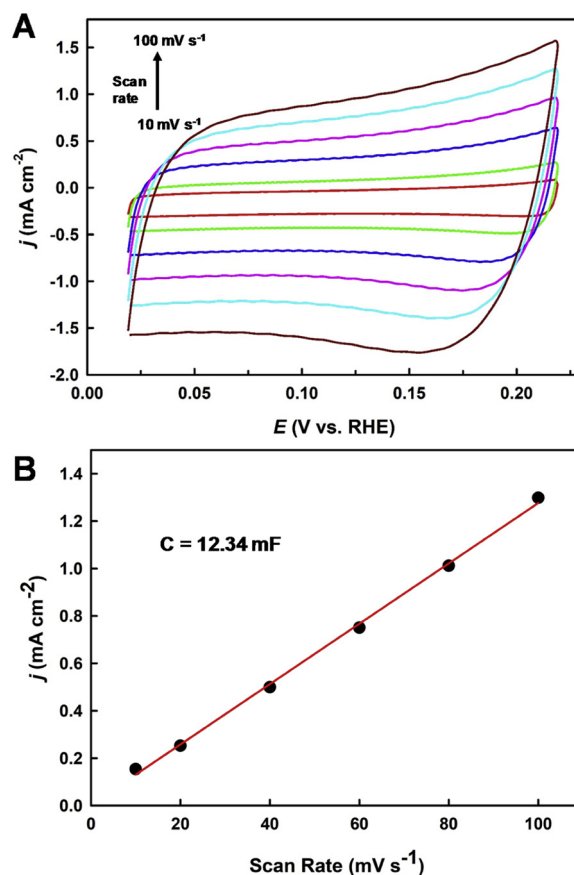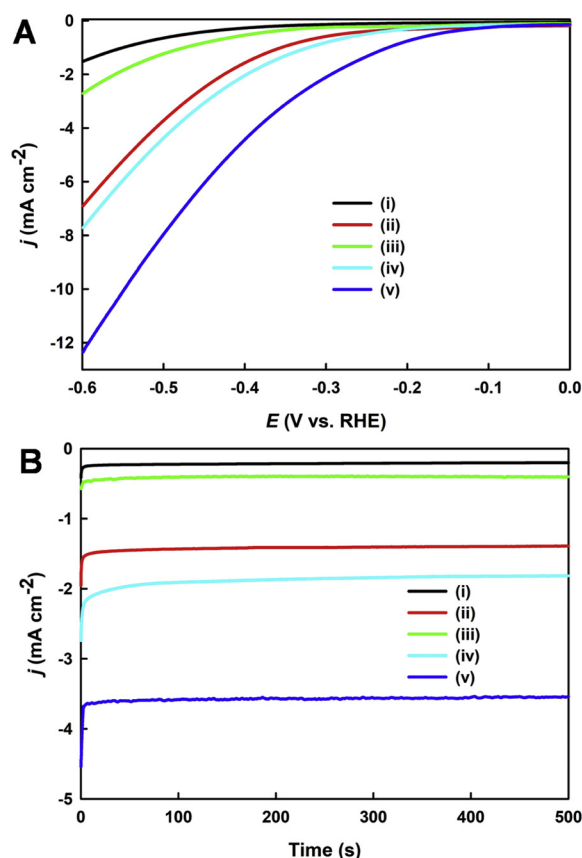

Fig. 3. Electrochemical surface area measurement of the Cu nanodendrites: (A) Determination of double-layer capacitance by CVs over a range of scan rates in a 0.1 M $HClO_4$ solution; (B) Corresponding current densities due to double-layer charging/discharging plotted against the potential scan rate.

high catalytic activity for CO_2 reduction. The formation of the Cu nanodendrites was also confirmed by the EDX analysis as shown in Fig. S2 (ii), where the O peak almost disappeared in comparison of Fig. S2 (i).

The crystalline phases of the formed different Cu electrodes were determined via XRD analysis as presented in Fig. 2A, revealing that they all had similar XRD patterns of pure Cu with a small amount of Cu_2O as specifically labelled. The small amount of Cu_2O might be resulted from the exposure to air. For comparison, Fig. S4 displays the XRD spectrum of the formed copper oxide nanodendrites, which was dramatically different from the spectrum of the Cu nanodendrites (Spectrum v of Fig. 2A). A number of CuO crystallite planes along with two small Cu_2O peak appeared, indicating that the calcination at 500 °C for 1 h was sufficient to convert Cu to copper oxide. Comparison of Fig. 2A and Fig.

S4 confirmed that the EC treatment could effectively reduce copper oxide to copper. All the Cu crystallite sizes (Table S1) were calculated based on the strongest Cu(111) peak using the Scherrer Equation, showing that Cu nanodendrites exhibited the smallest crystallite size. Figs. 2B and 2C depict the high-resolution Cu2p XPS spectrum of the formed copper oxide nanodendrites and Cu nanodendrites, respectively. The peak centered at 932.58 eV can be attributed to the Cu(I), whereas the peaks cantered at 934.88 and 936.07 eV corresponding to Cu(II) and two Cu(II) satellite peaks at higher binding energies of 941.48 and 944.35 eV appeared in Fig. 2B, indicating the formation of the copper oxides when the Cu thin film was calcinated at 500 °C for 1 h with a mixture of $CuSO_4$ and H_2SO_4 [42,43]. A strong peak centered at 932.30 eV attributed to Cu(0) associated with two Cu(II) oxide peaks at 934.22 and 935.86 eV and two Cu(II) weak satellite peaks were observed subsequent to the EC treatment as shown in Fig. 2C. The appearance of the strong Cu(0) peak in the Cu nanodendrite electrode confirmed that the EC treatment could effectively reduce copper oxide to copper, and the resulting oxides in the Cu nanodendrites might be resulted from air exposure during the XPS sample preparation [10].

The EASAs of the formed Cu thin film, OD-Cu thin film, and Cu nanodendrite electrodes were estimated relatively to a smooth polycrystalline Cu foil by measuring the double-layer capacitance in 0.1 M $HClO_4$ solution [27]. The CV of each electrode was recorded in the potential range, where no obvious Faradaic processes occurred, and the corresponding geometrical current density against the scan rate was plotted. The capacitance was calculated from the linear regression as shown in Fig. 3 and Fig. S5. The Cu nanodendrites exhibited the highest current density (Fig. 3A) at all the different scan rates compared to all the other Cu electrodes (Figs. S5A, S5C and S5E), indicating that Cu
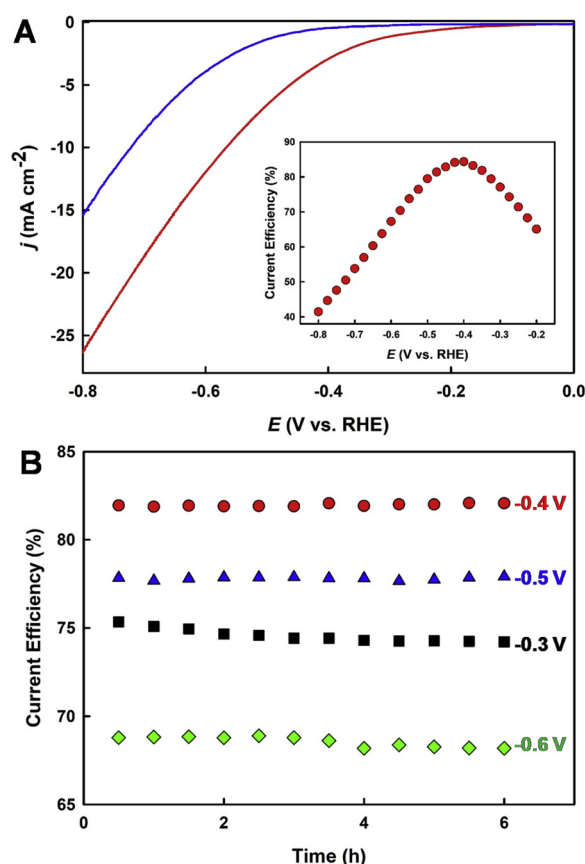
Fig. 4. (A) LSVs of different Cu electrodes recorded at 20 mVs^{-1}; (B) CA curves measured at -0.4 V for 500 s. Electrolyte: CO_2-saturated 0.1 M $NaHCO_3$ solution. Electrodes: (i) Cu thin film, (ii) OD-Cu thin film, (iii) Cu particles, (iv) Cu NPs, and (v) Cu nanodendrites.

Fig. 5. (A) LSVs of the Cu nanodendrites recorded in a Ar-saturated 0.1 M Na_2SO_4 solution (blue curve) and CO_2-saturated 0.1 M $NaHCO_3$ solution (red curve); the inset presents the corresponding instant current efficiency; and (B) Steady-state current efficiency (%) for CO_2 reduction at different applied cathodic potentials. (For interpretation of the references to colour in this figure legend, the reader is referred to the web version of this article).

nanodendrites possessed the largest double-layer capacitance. The current density was plotted against the scan rate for each electrode, showing a linear relationship. The plots were further fitted with high correlation coefficients (R^2) from 0.996 to 0.998. The capacitance was calculated from the slope of the linear regression, showing that the Cu nanodendrites achieved the highest double layer capacitance (Fig. 3B) compared to all the other Cu electrodes (Figs. S5B, S5D and S5F). The double-layer capacitance and the relative roughness factor of the different Cu-based electrodes were listed in Table S2, indicating that the Cu nanodendrite electrode possessed the highest EASA, which was 333 times higher than the smooth polycrystalline Cu plate. The EASA of the Cu thin film and OD-Cu thin film electrodes was 15 and 78 times higher than that of the smooth polycrystalline Cu plate, respectively.

3.2. Electrochemical activity

The electrocatalytic activity of the synthesized different Cu electrodes was initially studied by employing LSV and CA techniques in a CO_2-saturated 0.1 M $NaHCO_3$ (pH 6.65). Fig. 4A presents the LSV curves of the Cu-thin film, OD-Cu thin film, Cu particles, Cu NPs and Cu nanodendrites at the scan rate of 20 mV s^{-1}. The Cu nanodendrites demonstrated the highest current densities and earliest onset potential compared to all the other Cu electrodes. For instance, the cathodic current at -0.6 V of the Cu nanodendrites was measured to be 12.35 mA cm^{-2}, which was much higher than that of the Cu thin film (1.52 mA cm^{-2}), OD-Cu thin film (6.9 mA cm^{-2}), Cu particles (2.71 mA cm^{-2}), and Cu NPs (7.72 mA cm^{-2}). The steady-state current density of these electrodes was measured at -0.4 V and compared in CA curves (Fig. 4B), showing that the Cu nanodendrites achieved the highest current densities compared to all the other Cu electrodes. Both LSV and
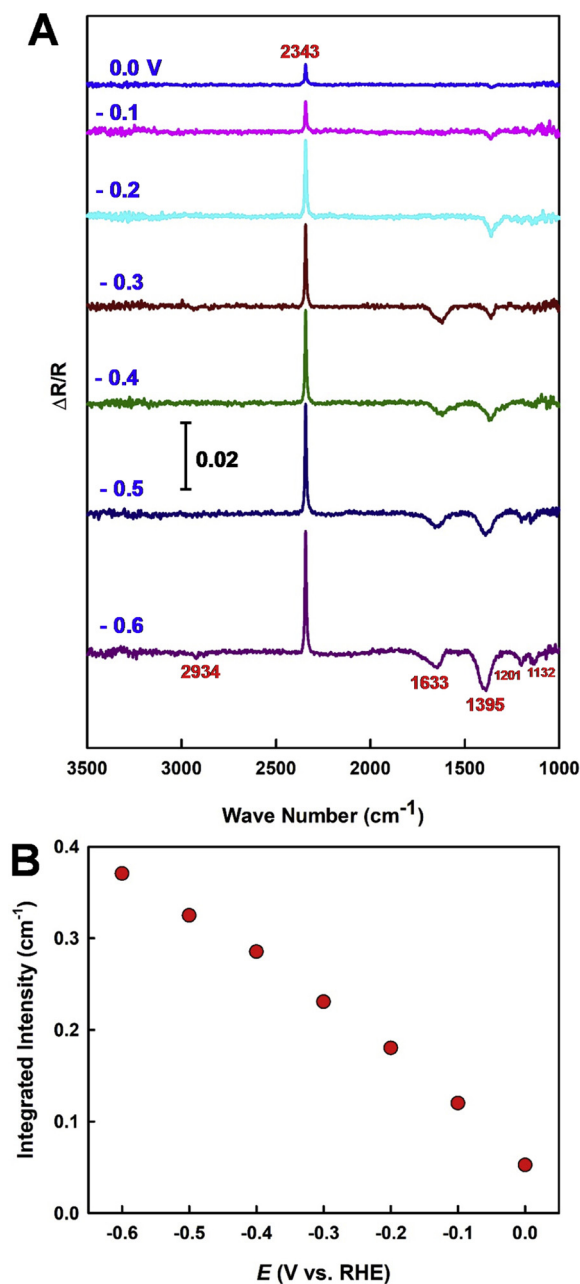
CA studies showed the superior electrocatalytic activity of the Cu nanodendrites in comparison to all other Cu electrodes fabricated in this study, indicating that the synthesized Cu nanodendrites might serve as a promising electrocatalyst for the CO_2 reduction.

In order to optimize the electrocatalytic activity of the Cu nanodendrites, various electrodes were synthesized and studied in terms of the volume of the mixture of the $CuSO_4$ and H_2SO_4 solution, the calcination temperature and the duration of annellation. Initially, the different amount of the mixture of 0.1 M $CuSO_4$ and 0.5 M H_2SO_4 was deposited on the Cu thin film during the calcination at 500 °C for 1 h, altered from 30 to 70 μL, showing that 50 μL deposition exhibited higher current densities in both the LSV and CA plots (Figs. S6A and S6B, respectively). The calcination temperature was further varied from 400 to 600 °C for 1 h by depositing the same amount of the $CuSO_4$ and H_2SO_4 mixture. It was shown that 500 °C was the optimal calcination temperature to form the highly active nanodendrites, which generated the highest current densities in the LSV and CA plots as seen in Figs. S6C and S6D. The effect of the duration of the calcination was further investigated, revealing that the highest catalytic activity was attained with the Cu nanodendrites grown at 500 °C for 60 min after depositing 50 μL of the $CuSO_4$ and H_2SO_4 mixture on the Cu thin film as observed in both the LSV (Fig. S6E) and CA (Fig. S6F) plots.

To further assess the electrocatalytic activity of the optimized electrode for the CO_2 reduction, LSVs were recorded in a CO_2-saturated 0.1 M $NaHCO_3$ (pH 6.65) as well as in an Ar-saturated 0.05 M Na_2SO_4 solution (pH was adjusted to be 6.65 by adding a small volume of 0.01 M H_2SO_4). As seen in Fig. 5A, the current density achieved in the

Fig. 6. (A) In situ electrochemical ATR-FTIR spectra for the CO_2 reduction at the Cu nanodendrites in a CO_2-saturated 0.1 NaHCO$_3$ solution at different applied potentials (vs. RHE); (B) Plot of the integrated infrared intensity of the CO_2 band centred at 2343 cm^{-1} vs the applied electrode potentials. The reference spectrum was taken at +0.2 V. For each spectrum, 32 scans were collected.

CO_2-saturated 0.1 M NaHCO$_3$ (red curve) was much higher than that in the Ar-saturated 0.1 M Na$_2$SO$_4$ (blue curve), indicating that the Cu nanodendrites exhibited a high catalytic activity toward the CO_2 reduction. The inset of Fig. 5A shows the corresponding ICE (%) for CO_2 reduction at the different applied potentials, which was calculated from the LSVs using the following equation [44]:
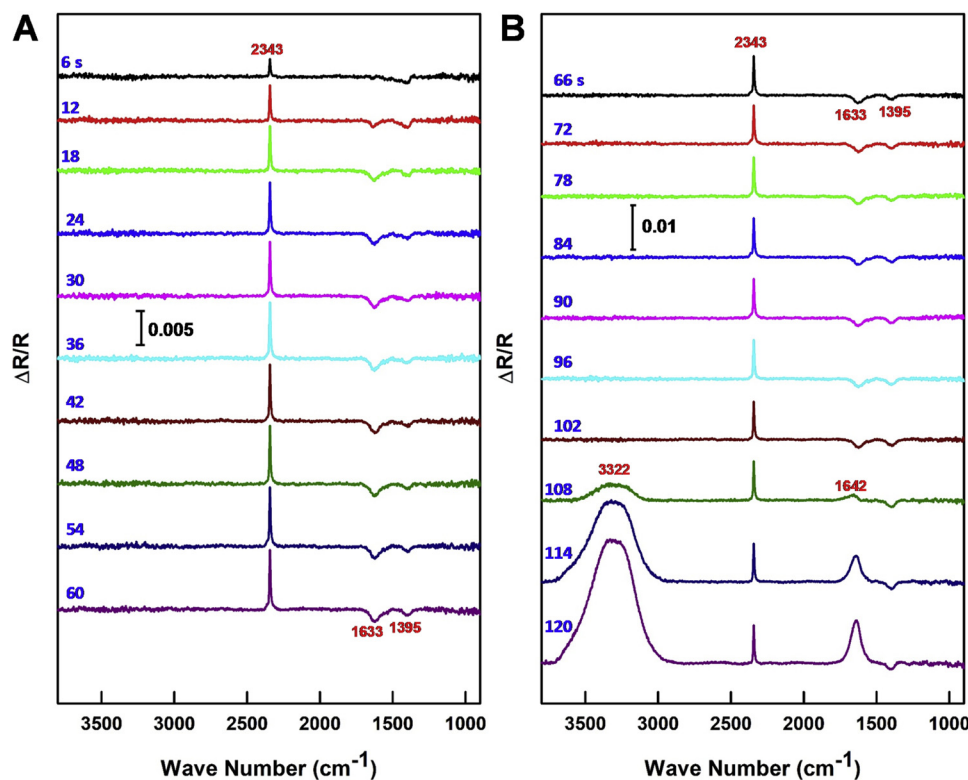
$$\text{ICE (\%)} = (j_C - j_A) \times 100 \, / \, j_C \quad (1)$$

where j_C was the current density obtained in the CO_2-saturated 0.1 M NaHCO$_3$ solution; and j_A was the current density measured in the Ar-saturated 0.05 M Na$_2$SO$_4$ solution. The ICE was gradually increased with the increase of the cathodic potential from -0.20 to -0.4 V;

however, it was decreased with the further increase of the cathodic potential from -0.4 to -0.8 V. The highest ICE (84.3%) was obtained at -0.4 V, which could be the optimal cathodic potential for the bulk electrolysis of CO_2 using the Cu nanodendrites. The SSCE for CO_2 reduction was further determined by employing CAs at the applied potential between -0.3 and -0.6 V over the 6 h electrolysis each. The CAs were recorded in both the CO_2-saturated 0.1 M NaHCO$_3$ and the Ar-saturated 0.05 M Na$_2$SO$_4$ (pH was adjusted to be 6.65) solutions, where CO_2 and Ar were continuously purged during the entire electrolysis, respectively. Fig. S7 presents the CA curve of the Cu nanodendrites for the electrochemical reduction of CO_2 at -0.5 V, where the current was almost constant during the entire electrolysis, indicating the high stability of the electrode. A high-resolution Cu2p XPS spectrum of the Cu nanodendrites after the electrochemical reduction of CO_2 was also recorded as displayed in Fig. S8. Comparison with Fig. 2C revealed that all the copper peaks were almost identical before and after the CO_2 reduction, further confirming the high stability of the formed Cu nanodendrites. Fig. 5B presents the steady-state current efficiency (SSCE), which was calculated using the Eq. (1). The overall SSCE was stable at all the applied potential. The SSCE was increased from 75.2% to 82.0% with the increase of the cathodic potential from -0.3 to -0.4 V. However, it was decreased from 77.8% to 68.5% with the further increase of the cathodic potential from -0.5 to -0.6 V, which is consistent with the ICE results (inset, Fig. 5A). Our GC analysis revealed that CO and CH$_4$ were the primary gas products for the CO_2 reduction at -0.6 V. The rates of the formation of CO and CH$_4$ were calculated to be 78.52 and 37.20 μmole cm^{-2} h^{-1}, respectively, which were very high in comparison with other copper-based nanostructured catalysts for the electrochemical reduction of CO_2 [7,44–47]. The performance of some promising Cu-based catalysts for the electrochemical reduction of CO_2 recently reported in the literature is compared in Table S3, showing that the novel Cu nanodendrites developed in the present study exhibited much higher current efficiency at a relatively low overpotential. All the aforementioned results indicated that the formed Cu nanodendrite is a promising catalyst for the electrochemical reduction of CO_2.

3.3. In situ electrochemical ATR-FTIR study

In situ ATR-FTIR spectroscopy was employed to detect the intermediates and products and to monitor the consumption of CO_2 during the electrochemical reduction of CO_2 on the Cu nanodendrites in a CO_2-saturated 0.1 M NaHCO$_3$ solutions. A schematic of the in-situ ATR-FTIR electrochemical cell set-up is shown in Scheme S1, where a ZnSe hemisphere crystal was used as the window. Fig. 6A displays a series of spectra as a function of potential with 0.1 V interval each, where a fresh CO_2-saturated solution was supplied to the electrode surface before the ATR-FTIR measurement at each applied electrode potential; and CO_2 was continuously purged into the solution. For each spectrum, 32 scans were collected, while the reference spectrum was recorded at +0.2 V (vs. RHE). As seen in Fig. 6A, a positive-going band centered at 2343 cm^{-1} appeared at all the applied potentials, which can be attributed to the CO_2 consumption [48,49]. As displayed in Fig. 6B, the integrated IR intensity of the CO_2 peak was gradually increased with the increase of the applied cathodic potentials, indicating that more CO_2 was reduced at the higher cathodic potential. A negative-going peak centered at 1395 cm^{-1} was observed in Fig. 6A, which can be ascribed to the IR absorption of HCO$_3^-$. The intensity of HCO$_3^-$ ions was increased with the increase of cathodic potential, indicating that more HCO$_3^-$ was formed at the higher cathodic potentials. A new downward peak centered at ~1633 cm^{-1} was observed at -0.3 V, which can be assigned to the asymmetric O−C=O stretching mode of HCOO$^-$ ions [50]. Two additional small negative-going peaks at ~1201 and ~1132 cm^{-1} appeared at -0.5 V (Fig. 6A), due to the bending of the C=O and C=O bonds formed during the electrochemical reduction of CO_2 on Cu nanodendrites [48]. Moreover, a small negative-going peak at 2933 cm^{-1} was noticed at -0.6 V, which could

Fig. 7. Time-resolved in situ ATR-FTIR spectra of CO_2 reduction on the Cu nanodendrites at -0.4 V (vs. RHE). (A) From 6 to 60 s; (B) from 66 to 120 s. The reference spectrum was taken at $+0.2$ V (vs. RHE). For each spectrum, 8 scans were collected.

be attribute to the asymmetric C—H stretching of the formed hydrocarbons [48,51]. For clarification, the IR spectra recorded at -0.4 and -0.6 V were enlarged and compared in Fig. S9, revealing the formation of hydrocarbons at the higher cathodic potential. To further identify those new products, we carried out NMR analysis. Fig. S10 displays the ^{1}H NMR spectrum of the formed liquid products from the CO_2 electrolysis at -0.6 V for 2 h, confirming the formation of $HCOO^-$, CH_3COO^- and CH_3OH.

As shown in Fig. 5, the highest current efficiency (over 80%) was attained at -0.4 V at the Cu nanodendrites. The in situ electrochemical ATR-FTIR spectroscopy was further employed to investigate the kinetics of the CO_2 reduction at this potential. A series of 20 spectra were recorded and presented in Fig. 7. It took 6 s to collect 8 scans for each spectrum. The strong positive-going peak centered at ~ 2343 cm^{-1} and the two negative-going peaks at 1395 and 1633 cm^{-1} were observed during the first 102 s, which is consistent with the results shown in Fig. 6A. However, it is interesting to note that two positive-going peaks centered at ~ 1642 and 3322 cm^{-1} appeared at 108 s, which could be assigned to the bond bending and stretching of a H_2O molecule, indicating the occurrence of water splitting. The intensity of the two peaks was significantly increased with the increase of the electrolysis time from 108 to 120 s. The aforementioned in situ ATR-FTIR results revealed that the solvated CO_2 was reduced at the Cu nanodendrites first; then the hydrogen evolution occurred when the solvated CO_2 molecules captured in the thin-layer between the electrode surface and the ZnSe hemisphere IR window were consumed. The novel design of the in situ ATR-FTIR system provided a facile approach to directly monitor the formation of the intermediates and products to study the mechanism and kinetics of the electrochemical CO_2 reduction at an electrode/electrolyte interface at a wide range of applied electrode potentials.

4. Conclusions

We have demonstrated a facile approach to synthesize novel oxide-derived Cu nanodendrites, which exhibited a high catalytic activity for the electrochemical reduction of CO_2. The unique Cu nanodendrites were directly grown when an electrodeposited Cu thin film was thermally treated at 500 °C in the presence of a mixture of $CuSO_4$ and H_2SO_4. The effect of applied cathodic potential on the electrochemical reduction of CO_2 at the Cu nanodendrites was systemically investigated by employing LSV and CA techniques, showing that the highest ICE (84.3%) and SSCE (82%) were attained at -0.4 V vs RHE. In situ electrochemical ATR-FTIR spectroscopy was employed to study the kinetics of the CO_2 reduction as a function of the applied electrode potential, while GC analysis and ^{1}H NMR spectroscopy were used to further identify the gas and liquid products, respectively, revealing that CO, CH_4, $HCOO^-$, CH_3COO^- and CH_3OH were formed. For the first time, our in-situ ATR-FTIR study provided the direct evidence, showing that the solvated CO_2 was electrochemically reduced first, and then the hydrogen evolution occurred when the solvated CO_2 molecules were consumed. This would have a significant implication of the system design for the efficient electrochemical reduction of CO_2. Our experimental results have also shown that the surface structure and the large electrochemically active surface area of the formed Cu nanodendrites played an important role in the efficient electrochemical reduction of CO_2. The facile fabrication, the unique nanodendritic structure, and the excellent catalytic activity make the Cu nanodendrites developed in this study as a promising electrocatalyst for the efficient conversion of CO_2 to usable products.

Declaration of Competing Interest

The authors declare no competing financial interest.

Acknowledgments

Appendix A. Supplementary data

Supplementary material related to this article can be found, in the online version, at doi:https://doi.org/10.1016/j.apcatb.2019.118096.

References

[1] M. Liu, Y. Pang, B. Zhang, P.D. Luna, O. Voznyy, J. Xu, X. Zheng, C.T. Dinh, F. Fan, C. Cao, F.P.G. de Arquer, T.S. Safaei, A. Mepham, A. Klinkova, E. Kumacheva, T. Filleter, D. Sinton, S.O. Kelley, E.H. Sargent, Enhanced electrocatalytic CO$_2$ reduction via field-induced reagent concentration, Nature 537 (2016) 382–386.

[2] M.N. Hossain, Z. Liu, J. Wen, A. Chen, Enhanced catalytic activity of nanoporous Au for the efficient electrochemical reduction of carbon dioxide, Appl. Catal. B: Environ. 236 (2018) 483–489.

[3] A.N. Marianov, Y. Jiang, Covalent ligation of Co molecular catalyst to carbon cloth for efficient electroreduction of CO$_2$ in water, Appl. Catal. B: Environ. 244 (2019) 881–888.

[4] Y. Hori, Electrochemical CO$_2$ reduction on metal electrodes, in: C.G. Vayenas, R.E. White, M.E. Gamboa-Aldeco (Eds.), Modern Aspects of Electrochemistry, Springer, New York, NY, 2008, pp. 89–189.

[5] D.M. Weekes, D.A. Salvatore, A. Reyes, A. Huang, C.P. Berlinguette, Electrolytic CO$_2$ reduction in a flow cell, Acc. Chem. Res. 51 (2018) 910–918.

[6] P. Lu, Y. Yang, J. Yao, M. Wang, S. Dipazir, M. Yuan, J. Zhang, X. Wang, Z. Xie, G. Zhang, Facile synthesis of single-nickel-atomic dispersed N-doped carbo framework for efficient electrochemical CO$_2$ reduction, Appl. Catal. B: Environ. 241 (2019) 113–119.

[7] M.N. Hossain, J. Wen, A. Chen, Unique copper and reduced graphene oxide nanocomposite toward the efficient electrochemical reduction of carbon dioxide, Sci. Rep. 7 (2017) 3184.

[8] R. Hegner, L.F.M. Rosa, F. Harnisch, Electrochemical CO$_2$ reduction to formate at indium electrodes with high efficiency and selectivity in pH neutral electrolytes, Appl. Catal. B: Environ. 238 (2018) 546–556.

[9] W. Sheng, S. Kattel, S. Yao, B. Yan, Z. Liang, C.J. Hawxhurst, Q. Wuc, J.G. Chen, Electrochemical reduction of CO$_2$ to synthesis gas with controlled CO/H$_2$ ratios, Energy Environ. Sci. 10 (2017) 1180–1185.

[10] C.W. Li, M.W. Kanan, CO$_2$ Reduction at low overpotential on Cu electrodes resulting from the reduction of thick Cu$_2$O films, J. Am. Chem. Soc. 134 (2012) 7231–7234.

[11] M. Dunwell, Q. Lu, J.M. Heyes, J. Rosen, J.G. Chen, Y. Yan, F. Jiao, B. Xu, The central role of bicarbonate in the electrochemical reduction of carbon dioxide on gold, J. Am. Chem. Soc. 139 (2017) 3774–3783.

[12] T.R. Cook, D.K. Dogutan, S.Y. Reece, Y. Surendranath, T.S. Teets, D.G. Nocera, Solar energy supply and storage for the legacy and nonlegacy worlds, Chem. Rev. 110 (2010) 6474–6502.

[13] D. Raciti, K.J. Livi, C. Wang, Highly dense Cu nanowires for low-overpotential CO$_2$ reduction, Nano Lett. 15 (2015) 6829–6835.

[14] T.T.H. Hoang, S. Ma, J.I. Gold, P.J.A. Kenis, A.A. Gewirth, Nanoporous copper films by additive-controlled electrodeposition: CO$_2$ reduction catalysis, ACS Catal. 7 (2017) 3313–3321.

[15] G. Keerthiga, B. Viswanathan, R. Chetty, Electrochemical reduction of CO$_2$ on electrodeposited Cu electrodes crystalline phase sensitivity on selectivity, Catal. Today 245 (2015) 68–73.

[16] Q. Zhai, S. Xie, W. Fan, Q. Zhang, Y. Wang, W. Deng, Y. Wang, Photocatalytic conversion of carbon dioxide with water into methane: platinum and copper(I) oxide co-catalysts with a core–shell structure, Angew. Chem. 125 (2013) 5888–5891.

[17] K. Manthiram, B.J. Beberwyck, A.P. Alivisatos, Enhanced electrochemical methanation of carbon dioxide with a dispersible nanoscale copper catalyst, J. Am. Chem. Soc. 136 (2014) 13319–13325.

[18] J.-F. Xie, Y.-X. Huang, W.-W. Li, X.-N. Song, L. Xiong, H.-Q. Yu, Efficient electrochemical CO$_2$ reduction on a unique chrysanthemum-like Cu nanoflower electrode and direct observation of carbon deposite, Electrochim. Acta 139 (2014) 137–144.

[19] Y. Wang, Z. Chen, P. Han, Y. Du, Z. Gu, X. Xu, G. Zheng, Single-atomic Cu with multiple oxygen vacancies on ceria for electrocatalytic CO$_2$ reduction to CH$_4$, ACS Catal. 8 (2018) 7113–7119.

[20] W. Luo, X. Nie, M.J. Janik, A. Asthagiri, Facet dependence of CO$_2$ reduction paths on Cu electrodes, ACS Catal. 6 (2016) 219–229.

[21] D. Kim, J. Resasco, Y. Yu, A.M. Asiri, P. Yang, Synergistic geometric and electronic effects for electrochemical reduction of carbon dioxide using gold–copper bimetallic Nanoparticles, Nature Commmun. 5 (2014) 4948.

[22] P. Hirunsit, Electroreduction of carbon dioxide to methane on copper, copper−silver, and copper−gold catalysts: a DFT study, J. Phys. Chem. C 117 (2013) 8262–8268.

[23] R. Reske, H. Mistry, F. Behafarid, B.R. Cuenya, P. Strasser, Particle size effects in the catalytic electroreduction of CO$_2$ on Cu nanoparticles, J. Am. Chem. Soc. 136 (2014) 6978–6986.

[24] W.J. Durand, A.A. Peterson, F. Studt, F. Abild-Pedersen, J.K. Norskov, Structure effects on the energetics of the electrochemical reduction of CO$_2$ by copper Surfaces, Surf. Sci. 605 (2011) 1354–1359.

[25] E. Bertheussen, A. Verdaguer-Casadevall, D. Ravasio, J.H. Montoya, D.B. Trimarco, C. Roy, S. Meier, J. Wendland, J.K. Nørskov, I.E.L. Stephens, I. Chorkendorff, Acetaldehyde as an intermediate in the electroreduction of carbon monoxide to ethanol on oxide-derived copper, Angew. Chem. Int. Ed. 55 (2016) 1450–1454.

[26] A. Dutta, M. Rahaman, N.C. Luedi, M. Mohos, P. Broekmann, Morphology matters: tuning the product distribution of CO$_2$ electroreduction on oxide-derived Cu foam catalysts, ACS Catal. 6 (2016) 3804–3814.

[27] C.W. Li, J. Ciston, M.W. Kanan, Electroreduction of carbon monoxide to liquid fuel on oxide-derived nanocrystalline copper, Nature 508 (2014) 504–507.

[28] D.W. Zhang, C.-H. Chen, J. Zhang, F. Ren, Fabrication of nanosized metallic copper by electrochemical milling process, J. Mater. Sci. 43 (2008) 1492–1496.

[29] A.J. Garza, A.T. Bell, M. Head-Gordon, Mechanism of CO$_2$ reduction at copper surfaces: pathways to C$_2$ products, ACS Catal. 8 (2018) 1490–1499.

[30] A. Wuttig, Y. Surendranath, Impurity ion complexation enhances carbon dioxide reduction catalysis, ACS Catal. 5 (2015) 4479–4484.

[31] J. Heyes, M. Dunwell, B. Xu, CO$_2$ Reduction on Cu at low overpotentials with surface-enhanced in situ spectroscopy, J. Phys. Chem. C 120 (2016) 17334–17341.

[32] A. Wuttig, C. Liu, Q. Peng, M. Yaguchi, C.H. Hendon, K. Motobayashi, S. Ye, M. Osawa, Y. Surendranath, Tracking a common surface-bound intermediate during CO$_2$-to fuels catalysis, ACS Cent. Sci. 2 (2016) 522–528.

[33] K.P. Kuhl, E.R. Cave, D.N. Abram, T.F. Jaramillo, New insights into the electrochemical reduction of carbon dioxide on metallic copper surfaces, Energy Environ. Sci. 5 (2012) 7050–7059.

[34] K.J.P. Schouten, Y. Kwon, C.J.M. van der Ham, Z. Qin, M.T.M. Koper, A new mechanism for the selectivity to C$_1$ and C$_2$ species in the electrochemical reduction of carbon dioxide on copper electrodes, Chem. Sci. 2 (2011) 1902–1909.

[35] X. Nie, M.R. Esopi, M.J. Janik, A. Asthagiri, Selectivity of CO$_2$ reduction on copper electrodes: the role of the kinetics of elementary steps, Angew. Chem. Int. Ed. 52 (2013) 2459–2462.

[36] A.A. Peterson, F. Abild-Pedersen, F. Studt, J. Rossmeisl, J.K. Norskov, How copper catalyzes the electroreduction of carbon dioxide into hydrocarbon fuels, Energy Environ. Sci. 3 (2010) 1311–1315.

[37] W. Tang, A.A. Peterson, A.S. Varela, Z.P. Jovanov, L. Bech, W.J. Durand, S. Dahl, J.K. Norskov, I. Chorkendorff, The importance of surface morphology in controlling the selectivity of polycrystalline copper for CO$_2$ electroreduction, Phys. Chem. Chem. Phys. 14 (2012) 76–81.

[38] Y. Hori, O. Koga, H. Yamazaki, T. Matsuo, Infrared spectroscopy of adsorbed CO and intermediate species in electrochemical reduction of CO$_2$ to hydrocarbons on a Cu electrode, Electrochim. Acta 40 (1995) 2617–2622.

[39] M.C. Figueiredo, I. Ledezma-Yanez, M.T.M. Koper, In situ spectroscopic study of CO$_2$ electroreduction at copper electrodes in acetonitrile, ACS Catal. 6 (2016) 2382–2392.

[40] A. Verdaguer-Casadevall, C.W. Li, T.P. Johansson, S.B. Scott, J.T. McKeown, M. Kumar, I.E.L. Stephens, M.W. Kanan, I. Chorkendorf, Probing the active surface sites for CO reduction on oxide-derived copper electrocatalysts, J. Am. Chem. Soc. 137 (2015) 9808–9811.

[41] B.D. Adams, R.M. Asmussen, C.K. Ostrom, A. Chen, Synthesis and comparative study of nanoporous palladium-based bimetallic catalysts for formic acid oxidation, J. Phys. Chem. C 118 (2014) 29903–29910.

[42] C.-K. Wu, M. Yin, S. O'Brien, J.T. Koberstein, Quantitative analysis of copper oxide nanoparticle composition and structure by X-ray photoelectron spectroscopy, Chem. Mater. 18 (2006) 6054–6058.

[43] I. Platzman, R. Brener, H. Haick, R. Tannenbaum, Oxidation of polycrystalline copper thin films at ambient conditions, J. Phys. Chem. C 112 (2008) 1101–1108.

[44] M.N. Hossain, J. Wen, S.K. Konda, M. Govindhan, A. Chen, Electrochemical and FTIR spectroscopic study of CO$_2$ reduction at a nanostructured Cu/reduced graphene oxide thin film, Electrochem. Commun. 82 (2017) 16–20.

[45] J. Qiao, Y. Liu, F. Hong, J. Zhang, A review of catalysts for the electroreduction of carbon dioxide to produce low-carbon fuels, Chem. Soc. Rev. 43 (2014) 631–675.

[46] M. Fan, Z. Bai, Q. Zhang, C. Ma, X.-D. Zhou, J. Qiao, Aqueous CO$_2$ reduction on morphology controlled Cu$_x$O nanocatalysts at low overpotential, RSC Adv. 4 (2014) 44583–44591.

[47] H. Mistry, R. Reske, P. Strasser, B.R. Cuenya, Size-dependent reactivity of gold-copper bimetallic nanoparticlesduring CO$_2$ electroreduction, Catal. Today 288 (2017) 30–36.

[48] B. Innocent, D. Pasquier, F. Ropital, F. Hahn, J.-M. Le´ger, K.B. Kokoh, FTIR spectroscopy study of the reduction of carbon dioxide on lead electrode in aqueous medium, Appl. Catal. B: Environ. 94 (2010) 219–224.

[49] J. Wang, R.M. Asmussen, B. Adams, D.F. Thomas, A. Chen, Facile synthesis and electrochemical properties of intermetallic PtPb nanodendrites, Chem. Mater. 21 (2009) 1716–1724.

[50] B.D. Mistry, A Handbook of Spectroscopic Data Chemistry (UV, IR, PMR, 13CNMR and Mass Spectroscopy), Edition oxford book company, Jaipur, India, 2009, pp. 36–44.

[51] R. Ortiz, O.P. Mfirquez, J. Mfirquez, C. Gutierrez, FTIR spectroscopy study of the electrochemical reduction of CO$_2$ on various metal electrodes in methanol, J. Electroanal. Chem. 390 (1995) 99–107.